

Three-Dimensional Nonlinear Dynamics of Thin Liquid Films

Alexander Oron*

*Department of Mechanical Engineering, Technion-Israel Institute of Technology,
Haifa 32000, Israel*

(Received 8 March 2000)

Three-dimensional dynamics of thin Newtonian liquid films subjected to long-range van der Waals forces on a horizontal coated solid surface is numerically studied in the framework of the long-wave theory. The dynamics of nonvolatile films results in the emergence of an isolated steady drop standing on a practically flat film, while volatile films uniformly disappear on the macroscale. In both cases the evolution of the initial small-amplitude noise spans over the stages of self-organization, fast thinning of the depressions, formation and expansion of the “holes,” emergence of the polygonal network of liquid ridges, and its breakup, as seen in the experiments.

PACS numbers: 47.20.-k, 68.10.Jy, 68.15.+e

The subject of dewetting of solid surfaces by ultrathin liquid films has received wide interest in recent years. Experiments were carried out to study the pattern formation in the process of dewetting mainly by polymer nonvolatile [1–4] films and their volatile aqueous solutions [5]. These experiments show that in the nonvolatile case the film typically evolves through the stages of emergence of holes, their expansion and coalescence, formation of a polygonal network of liquid ridges, and its breakup into spherical drops. In the volatile case the emergence of a polygonal network is representative, when slow evaporation takes place. Theoretical work is as a rule based on the long-wave theory of thin liquid films [6] and is carried out for Newtonian nonevaporating [7–9] and evaporating films [10,11]. Surprisingly enough the comparison between such theoretical predictions and experimental observations made for polymer films is favorable [3,4]. The vast majority of the theoretical work is done for two-dimensional (2D) films whose dynamics is governed by a 1D in space evolution equation. However, investigations of the dynamics of 3D films via numerical studies of the pertinent 2D in space evolution equations now appear in the literature. Khanna and Sharma studied the evolution of thin nonvolatile films with the Lennard-Jones 3-9 potential used for apolar films [8] and the potential involving long-range apolar van der Waals repulsion and short-range hydrophobic attraction employed for aqueous films [9]. The first case showed the emergence of patterns of holes, while in the second case two different kinds of pattern formations were encountered: (i) for relatively thick (>8 nm in the example [9]) films it engenders the formation of isolated circular holes; (ii) for thinner (<8 nm [9]) films it leads to the emergence of isolated droplets.

One purpose of this paper is to study the dynamics of a 3D ultrathin apolar Newtonian liquid film on a coated surface and to investigate the pattern formation associated with it. Existing 2D studies can provide general qualitative information about the film evolution and its outcome, but not a detailed understanding of the process—thus the

novelty of the results given here. A liquid film of the average thickness d , viscosity μ , density ρ , kinematic viscosity $\nu = \mu/\rho$, surface tension σ , and thermal conductivity k_{th} is considered on a solid substrate coated with a solid layer of thickness $\delta \ll d$ and held at the uniform temperature ϑ_w . The film thickness is assumed in the range ~ 100 nm, where intermolecular London–van der Waals dispersion forces are effective, and they are taken into account, while thermocapillarity and gravity are neglected. Evaporation of the film is accounted for in the framework of a one-sided model derived by Burelbach *et al.* [12] with the effect of vapor recoil neglected. Further details can be found in [6,11].

To describe the evolution of the film on a coated solid surface the dimensionless scaled potential adopted for the intermolecular interactions is written in the form [11] $\Phi = (A/3)h^{-3} - (B/4)h^{-4}$, where $h = h(x, y, \tilde{t})$ is the film thickness, as normalized with respect to d , x, y are the spatial coordinates in the plane of the substrate scaled with d , \tilde{t} is the time scaled with d^2/ν , and A, B are positive Hamaker constants defined below, Eq. (4), all dimensionless. This potential was derived [11] by expanding the appropriate composite potential [13] resulting from the pertinent interaction between four phases, i.e., solid, coating, liquid, and gas. The form of Φ , which is similar to Lennard-Jones 3-9 potential [14], suggests that the dispersion forces are attractive for larger film thicknesses and repulsive for smaller ones.

The long-wave evolution equation describing the spatio-temporal dynamics of an evaporating thin liquid film subjected to the intermolecular interactions of the type described above and capillary forces is given as [6,11]

$$h_t + \frac{\bar{E}}{h + K} + \nabla \cdot \left(-h^3 \frac{d\Phi}{dh} \nabla h + Wh^3 \nabla \nabla^2 h \right) = 0 \quad (1)$$

with periodic boundary conditions in the domain $0 \leq x \leq \bar{L}_x$, $0 \leq y \leq \bar{L}_y$. Here the parameters of the problem are

given by

$$W = \frac{3\epsilon^3 \sigma d}{\rho \nu^2}, \quad \bar{E} = \epsilon^{-1} \frac{k_{\text{th}}(\vartheta_s - \vartheta_w)}{\rho \nu \mathcal{L}}, \quad (2)$$

$$K = \frac{\vartheta_s^{3/2} k_{\text{th}}}{\hat{\alpha} \rho_g \mathcal{L}^2 d} \left(\frac{2\pi R_g}{M_w} \right)^{1/2}$$

that represent the inverse capillary number, the evaporation number, and the interfacial resistance to phase change, respectively, ϵ is the small parameter of the long-wave expansion [6], $t = \epsilon \tilde{t}$, ϑ_s is the ambient saturation temperature, \mathcal{L} is the latent heat of evaporation, R_g is the universal gas constant, ρ_g is the vapor density, M_w is the molecular weight of the liquid, and $\hat{\alpha}$ is the accommodation coefficient [12].

In the case of a nonevaporating film ($E = 0$) the linear stability analysis of a uniform state $h = 1$ perturbed by an infinitesimal disturbance $\sim \exp(\omega t + ik_x x + ik_y y)$ yields the characteristic equation $\omega = (A - B)k^2 - Wk^4$, where $k = (k_x^2 + k_y^2)^{1/2}$ is a wave number of the disturbance and ω is its growth rate. The fastest growing mode is given by the wave number $k_m = [(A - B)/2W]^{1/2}$ and the wavelength $L_m = 2\pi/k_m$. In the computations presented below the lateral size of the periodic domain is taken to be as large as $2L_m$ and higher.

In the nonevaporating case the system (1) has the Lyapunov functional [11] $\mathcal{F} = \int [V(h) + W|\nabla h|^2/2] dx dy$ with the ‘‘potential’’ $V(h) = \int \Phi dh = Bh^{-3}/12 - Ah^{-2}/6$. Because of this fact the minimal value of the solution is expected to roughly correspond to the location of the minimal value of $V(h)$, i.e., $h = h_m = 3B/4A$. Thus the true dewetting does not occur, even, as we shall see, when evaporation takes place. We refer hereafter to the deep depressions in the film interface when the corresponding local thickness $h \approx h_m$ as ‘‘holes.’’

Equation (1) is rescaled to the form

$$h_\tau + \frac{E}{h + K} + \nabla \cdot [(\gamma h^{-1} - h^{-2})\nabla h + h^3 \nabla \nabla^2 h] = 0 \quad (3)$$

to be solved in the domain $\Omega = [0, L_x] \times [0, L_y]$, where the new spatial coordinates are stretched by $\sqrt{B/W}$ with respect to the old ones, $\tau = B^2 t/W$, $E = \bar{E}W/B^2$, $L_x = \bar{L}_x \sqrt{B/W}$, $L_y = \bar{L}_y \sqrt{B/W}$, and $\gamma = A/B$. The initial data $h = h_0(x, y)$ used here is a small-amplitude pseudo-random perturbation of the uniform state $h = 1$.

The numerical technique used here to solve Eq. (3) is based on the Newton-Kantorovich method, as described by Oron [15]. Equation (3) is rewritten in the form $h_\tau + F(h) = 0$ and linearized using the Frechet derivative of the operator F . As a result of linearization and discretization in time, a linear partial differential equation (PDE) in two spatial dimensions is obtained and is further discretized using a finite differencing scheme based on a spatially uniform staggered grid accurate to $O(\Delta x^2 + \Delta y^2)$. The evaluation of the Frechet derivatives and the finite difference dis-

cretization are carried out in the conservative form using linear interpolation for half nodes, so that for a nonvolatile film its total mass is conserved up to $O(10^{-12})\%$ of the initial value. The sets of linear algebraic equations arising from discretization of the PDE are solved iteratively using the ITPACK package, when the convergence at each time step is achieved with the tolerance error of $O(10^{-12})$. As an additional check for accuracy of the numerical solution, the value of the Lyapunov functional for a nonvolatile film is computed at each time step, and its monotonic decrease is verified. The time-marching technique is a modified Euler method accurate to $O(\Delta t^2)$. The grid of 51×51 was used below to compute the solutions for Eq. (3) in square periodic domains.

As an example for our numerical study we choose an octane (or other typical hydrocarbon liquid) layer on a silicon wafer coated by fused quartz and bounded by air. The Hamaker constants for these four phases (s , substrate; c , coating; l , liquid; g , gas) are given [16] as $A_s = 44.0 \times 10^{-20}$ J, $A_c = 6.3 \times 10^{-20}$ J, $A_l = 4.5 \times 10^{-20}$ J, $A_g \approx 0$. The constants α_1 and α_2 are calculated [11]: $\alpha_1 = (A_s^{1/2} - A_c^{1/2})(A_l^{1/2} - A_g^{1/2}) \approx 8.75 \times 10^{-20}$ J; $\alpha_2 = (A_c^{1/2} - A_l^{1/2})(A_g^{1/2} - A_l^{1/2}) \approx -0.82 \times 10^{-20}$ J. The coefficients A, B are defined as [11]

$$A = \frac{\epsilon(\alpha_1 + \alpha_2)}{2\pi \rho \nu^2 d}, \quad B = \frac{2\epsilon \delta \alpha_1}{\pi \rho \nu^2 d^2}, \quad (4)$$

and $\gamma \equiv A/B = (1 + \alpha_2/\alpha_1)/4(\delta/d)$. For a given choice of the four substances the parameter γ varies around the value of 3, when the coating thickness is below one-tenth of the film thickness. In contrast with the free energy potential used in [9] which admits instability for a certain range of film thickness, our potential of intermolecular interactions prescribes instability for thick films and stability for thin ones, i.e., long-range attractions and short-range repulsions.

The film dynamics is shown in the figures below in the form of contour and surface plots in continuous gray scale, when the bright and dark shades correspond to higher and lower elevations, respectively. A typical evolution of a nonvolatile film, as presented in Fig. 1, exhibits several stages. Driven by initial instability of the film several depressions emerge [five depressions in snapshot (a)] and rapidly deepen leading to formation of holes that reach the depth roughly corresponding to the minimum of the appropriate potential energy at $h = h_m$ [snapshot (b)]. These circular holes then expand and coalesce driving the fluid away from the holes into the liquid ridges which form a nearly polygonal network [snapshots (c) and (d)]. It is interesting to compare this pattern with the experimental patterns observed by Sharma and Reiter [3] (see their Figs. 7 and 8 to find similarity). The morphology of the ridges with elevated vertices and uneven rims is also similar to that found in the experiments [3] (see their Figs. 3 and 5).

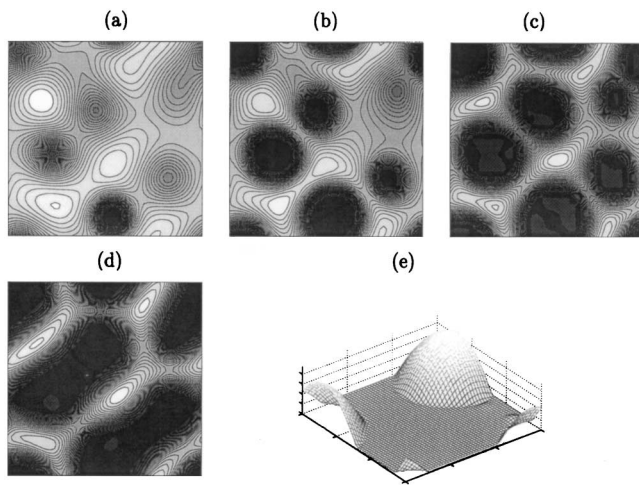


FIG. 1. The evolution of the nonevaporating film as described by Eq. (3) with $\gamma = 3$, $E = 0$ and the initial data given by the random perturbation of $h = 1$ with the amplitude of 0.05. The periodic domain is $L_x = L_y = 15$. x and y are dimensionless spatial coordinates that represent the respective physical spatial variables scaled with $\epsilon^{-1}d\sqrt{B/W}$. The consecutive snapshots correspond to $\tau =$ (a) 4.602, (b) 5.102, (c) 5.602, (d) 6.602 (contour plots), and (e) 17.572 (surface plot). The maximum and minimum elevations of the interface (h_{\max}, h_{\min}) are, respectively, (1.2922, 0.2785), (1.6139, 0.2480), (2.0505, 0.2246), (2.3300, 0.2335), and (4.7915, 0.2092). A polygonal network of liquid ridges qualitatively similar to the experimental observations made by Sharma and Reiter [3] is seen in snapshots (b)–(d). Bright and dark shades correspond to elevations and depressions, respectively.

Further expansion of the holes leads to their further coalescence, breakup of the ridges, and formation of oblique structures that consist of almost flat valleys and ridges (not shown). The liquid ridges disintegrate into

separate elongated drops (not shown) which finally aggregate to a single drop that becomes axisymmetric [snapshot (e)]. We find that for all used sizes of the periodic domain the final state is an isolated drop sitting on top of a thin, fairly flat wetting layer. This result is in agreement with the conclusions drawn by Mitlin [14] in the 2D case that the coarsening dynamics leads to the emergence of a single-hump structure and with mathematical statements [17]. This 3D evolution, as presented here, constitutes a generalization of the 2D film dynamics under the identical form of the potential [11].

A representative example of the evolution of a slowly evaporating film is presented in Fig. 2, where the parameters of the problems are chosen identical to those used for a nonvolatile film in Fig. 1 except for $E = 0.2$, $K = 1$. The stages of the evolution, as seen in Fig. 2, are self-organization of the pattern and formation of peaks and troughs [snapshot (a)], formation of deep circular troughs and their broadening [snapshot (b)], expansion of the holes and formation of a polygonal network of liquid ridges [snapshot (c)], further expansion of the holes, breakup of the network [snapshot (d)], and the emergence of isolated ridges [snapshot (e)]. These ridges decrease in height not due to evaporation, but because they feed the liquid into the shallow plateau on top of which they stand. This effect described here in 3D is similar to what was found and discussed in the 2D case by Oron and Bankoff [11], and the reader is referred there for more details. Along with their decay in height the ridges become, primarily due to the capillary forces, increasingly symmetric [snapshots (f)–(h)]. Once the height of the drops decreases to the thickness of the plateau, the liquid remaining rapidly dries out almost uniformly in space. It is emphasized that during the film evolution the holes interact and coalesce, thus

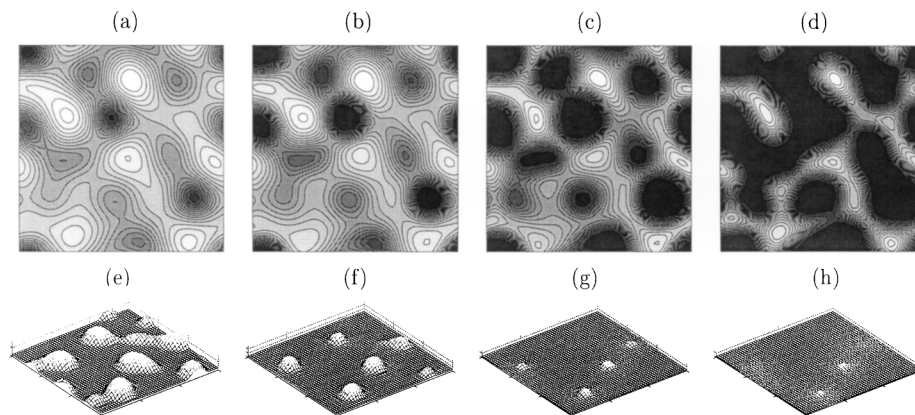


FIG. 2. The evolution of the evaporating film as described by Eq. (3) with $\gamma = 3$, $E = 0.2$, $K = 1$ and the initial data given by the random perturbation of $h = 1$ with the amplitude of 0.05. The periodic domain is $L_x = L_y = 15$. x and y are dimensionless spatial coordinates that represent the respective physical spatial variables scaled with $\epsilon^{-1}d\sqrt{B/W}$. The consecutive snapshots correspond to $\tau =$ (a) 2.2, (b) 2.4, (c) 2.6, (d) 3.0 (contour plots) and $\tau =$ (e) 3.8, (f) 4.7, (g) 5.1, (h) 5.2 (surface plots). The maximum and minimum elevations of the interface (h_{\max}, h_{\min}) are, respectively, (0.9239, 0.3588), (1.0326, 0.2808), (1.3031, 0.2518), (1.7323, 0.2178), (1.7512, 0.2136), (1.3869, 0.1704), (0.8227, 0.1506), and (0.5054, 0.1387). After $\tau = 5.2$ the film rapidly flattens out and evaporates uniformly. A polygonal network of liquid ridges qualitatively similar to the experimental observations made by Thiele *et al.* [5] is seen in snapshot (c). Bright and dark shades correspond to elevations and depressions, respectively.

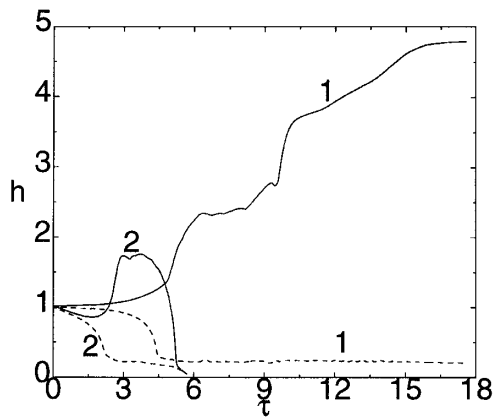


FIG. 3. The time evolution of the maximal h_{\max} (solid lines) and minimal h_{\min} (broken lines) elevations of the interface in the cases presented in Figs. 1 and 2. The corresponding curves are marked, respectively, by 1 and 2.

leading to the breakup of the polygonal structure in contrast with the observations of Thiele *et al.* [5] in their experiments with aqueous solutions of collagen. The persistence of the polygonal network of liquid ridges there is explained by the presence of collagen. The dynamics of films evaporating at a higher rate, e.g., $E > 0.6$, with $K = 1$ leads to flattening out of the film much before approaching the critical thickness of $h = h_m$ and then to rapid dryout.

The temporal dynamics of the maximal and minimal values of h , respectively, h_{\max} and h_{\min} in both cases presented in Figs. 1 and 2 is shown in Fig. 3. The rate of film thinning in both nonvolatile and volatile cases significantly diminishes, when h_{\min} approaches the value of 0.25 for a used value of γ . The time range corresponding to the steep decrease of the h_{\max} curve and to a fairly slow decrease of h_{\min} in the evaporating case, as shown in Fig. 3, corresponds to the “feeding” or “reservoir” effect addressed above. The complex behavior of h_{\max} in case 1 is associated with the merging of adjacent drops.

Finally, 3D computations presented for nonvolatile films show that a use of the potential Φ employed here instead of the Lennard-Jones potential [8] leads to the formation of “drop patterns” instead of “hole patterns” observed there, despite the topological similarity between the two potentials. The reason for this profound difference is related to the disparity between the minimal thicknesses h_m of the film in the two cases. While in our theory h_m is determined directly from the values A and B , Khanna and Sharma [8] calculated their A and B such that the dimensional value

of h_m (their l_0) = 0.137 nm, which is outside the range of continuum theory and certainly much smaller than our $h_m \approx 25$ nm. The existence of a “thick” microlayer facilitates a relatively free liquid flow along the coated substrate and the accumulation of the liquid in an isolated drop standing on a plateau minimizing by that the free energy of the system.

The author thanks Professor S.G. Bankoff for useful comments and Mr. R. Gabay for his help with computing matters. The research was partially supported by Grant No. 96-395 from the United States–Israel Binational Science Foundation (BSF), Jerusalem, Israel.

*Electronic address: meroron@tx.technion.ac.il

- [1] C. Redon, F. Brochard-Wyart, and F. Rondelez, *Phys. Rev. Lett.* **66**, 715 (1991).
- [2] G. Reiter, P. Auroy, and L. Auvray, *Macromolecules* **29**, 2150 (1996).
- [3] A. Sharma and G. Reiter, *J. Colloid Interface Sci.* **178**, 383 (1996).
- [4] R. Xie *et al.*, *Phys. Rev. Lett.* **81**, 1251 (1998).
- [5] U. Thiele, M. Mertig, and W. Pompe, *Phys. Rev. Lett.* **80**, 2869 (1998).
- [6] A. Oron, S.H. Davis, and S.G. Bankoff, *Rev. Mod. Phys.* **69**, 931 (1997).
- [7] R. Khanna, A. T. Jameel, and A. Sharma, *Ind. Eng. Chem. Res.* **35**, 3081 (1996).
- [8] R. Khanna and A. Sharma, *J. Colloid Interface Sci.* **195**, 42 (1997).
- [9] A. Sharma and R. Khanna, *Phys. Rev. Lett.* **81**, 3463 (1998); *J. Chem. Phys.* **110**, 4929 (1999).
- [10] A.S. Padmakar, K. Kargupta, and A. Sharma, *J. Chem. Phys.* **110**, 1735 (1999).
- [11] A. Oron and S.G. Bankoff, *J. Colloid Interface Sci.* **218**, 152 (1999); A. Oron and S.G. Bankoff, in *Non-linear Singularities in Deformation and Flow*, edited by D. Durban and J.R.A. Pearson (Kluwer, Dordrecht, 1999), p. 339.
- [12] J.P. Burelbach, S.G. Bankoff, and S.H. Davis, *J. Fluid Mech.* **195**, 463 (1988).
- [13] G.J. Hirasaki, in *Interfacial Phenomena in Petroleum Recovery*, edited by N.R. Morrow (Marcel Dekker, New York, 1991).
- [14] V.S. Mitlin, *J. Colloid Interface Sci.* **156**, 491 (1993); V.S. Mitlin and N.V. Petviashvili, *Phys. Lett. A* **192**, 323 (1994).
- [15] A. Oron, *Phys. Fluids* **12**, 1633 (2000).
- [16] J.N. Israelachvili, *Intermolecular and Surface Forces* (Academic Press, London, 1992).
- [17] A.B. Givental, *Theor. Math. Phys.* **76**, 76 (1989).